

## Lecture 4: Mechanical Alloying, Case Study

### Introduction

An alloy can be created without melting, by violently deforming mixtures of different powders, Fig. 1. Inert oxides can, using this technique, be introduced uniformly into the microstructure. The dispersion-strengthened alloyed powders are then consolidated using hot-isostatic pressing and extrusion, to produce a solid with a very fine grain structure. Heat treatment then induces recrystallisation, either into a coarse columnar grain structure or into a fine, equiaxed set of grains.

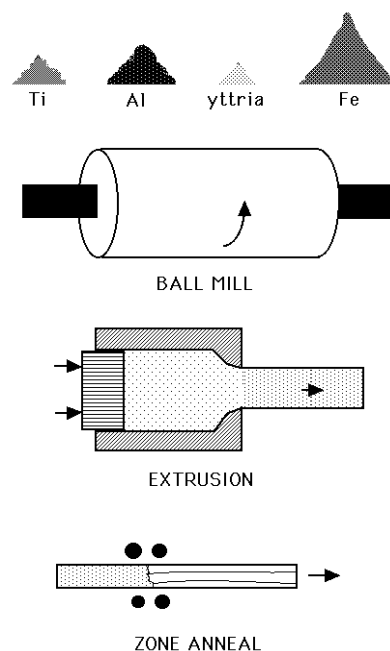


Fig. 1: The manufacture of mechanically alloyed metals for engineering applications. The elemental powders/master-alloys/oxides are milled together to produce solid solutions with uniform dispersions of oxide particles. This powder is consolidated and the resulting material heat-treated to achieve a coarse, directional grain structure.

The chemical compositions of some of the commercial alloys produced using this method are listed in Table 1. They all contain chromium and/or aluminium for corrosion and oxidation resistance, and yttrium or titanium oxides for creep strength.

### CHEMICAL STRUCTURE

The intense deformation associated with mechanical alloying can force atoms into positions where they may not prefer to be at equilibrium. The atomic structure of

Fe-base	C	Cr	Al	Mo	Ti	N		Ti <sub>2</sub> O <sub>3</sub>	Y <sub>2</sub> O <sub>3</sub>	Fe
MA956	0.01	20.0	4.5	–	0.5	0.045		–	0.50	Balance
PM2000	< 0.04	20.0	5.5		0.5			–	0.5	Balance
Ni-Base	C	Cr	Al	Ti	W	Fe	N	Total O	Y <sub>2</sub> O <sub>3</sub>	Ni
MA6000	0.06	15.0	4.5	2.3	3.9	1.5	0.2	0.57	1.1	Balance
PM1000 †		20.0	0.3	0.5		3.0			0.6	Balance

Table 1: Compositions (wt% ) of some typical alloys.

solid solutions in commercially important metals formed by the mechanical alloying process can be studied using field ion microscopy and the atom-probe.

A solution which is homogeneous will nevertheless exhibit concentration differences of increasing magnitude as the size of the region which is chemically analysed decreases. These are random fluctuations which obey the laws of stochastic processes, and represent the real distribution of atoms in the solution. These equilibrium variations cannot usually be observed directly because of the lack of spatial resolution and noise in the usual microanalytical techniques. The fluctuations only become apparent when the resolution of chemical analysis falls to less than about a thousand atoms block. The atom probe technique collects the experimental data on an atom by atom basis. The atom by atom data can be presented at any block size.

Fig. 2 illustrates the variation in the iron and chromium concentrations in fifty atom blocks, of the ferrite in *MA956*. There are real fluctuations but further analysis is needed to show whether they are beyond what is expected in homogeneous solutions

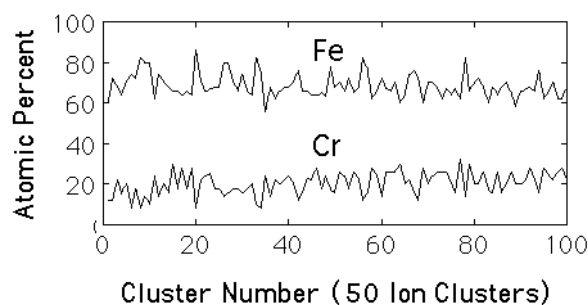


Fig. 2: The variation in the iron and chromium concentrations of 50 atom samples of MA956.

For a random solution, the distribution of concentrations should be binomial since the fluctuations are random; any significant deviations from the binomial distribution would indicate either the clustering of like-atoms or the ordering of unlike pairs.

The frequency distribution is obtained by plotting the total number of composition blocks with a given number of atoms of a specified element against the concentration.

Fig. 3 shows that the experimental distributions are essentially identical to the calculated binomial distributions, indicating that the solutions are random.

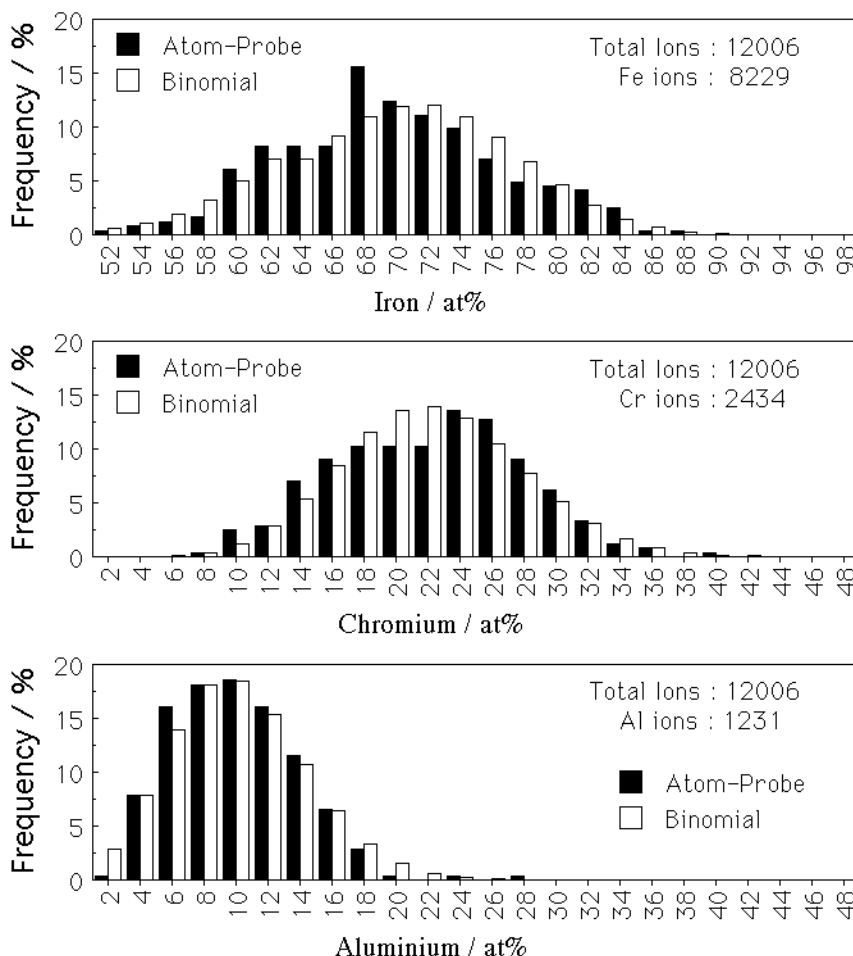


Fig. 3: Frequency distribution curves for iron, chromium and aluminium in mechanically alloyed MA956.

This does not mean that the solutions are thermodynamically ideal, but rather that the alloy preparation method which involves intense deformation forces a random dispersal of atoms. Indeed, Fe–Cr solutions are known to deviate significantly from ideality, with a tendency for like atoms to cluster. Thus, it can be concluded that the alloy is in a mechanically homogenised nonequilibrium state, and that prolonged annealing at low temperatures should lead to, for example, the clustering of chromium atoms.

### Solution Formation

Normal thermodynamic theory for solutions begins with the mixing of component atoms. In mechanical alloying, however, the solution is prepared by first mixing together lumps of the components, each of which might contain many millions of identical atoms. We examine here the way in which a solution evolves from these large

lumps into an intimate mixture of different kinds of atoms without the participation of diffusion or of melting. It will be shown later that this leads to interesting outcomes which have implications on how we interpret the mechanical alloying process.

Consider the pure components  $A$  and  $B$  with molar free energies  $\mu_A^o$  and  $\mu_B^o$  respectively. If the components are initially in the form of powders then the average free energy of such a mixture of powders is simply:

$$G\{\text{mixture}\} = (1-x)\mu_A^o + x\mu_B^o \quad (1)$$

where  $x$  is the mole fraction of  $B$ . It is assumed that the powder particles are so large that the  $A$  and  $B$  atoms do not “feel” each other’s presence via interatomic forces between unlike atoms. It is also assumed that the number of ways in which the mixture of powder particles can be arranged is not sufficiently different from unity to give a significant contribution to a configurational entropy of mixing. Thus, a blend of powders which obeys equation 1 is called a *mechanical mixture*. It has a free energy that is simply a weighted mean of the components, as illustrated in Fig. 4a for a mean composition  $x$ .

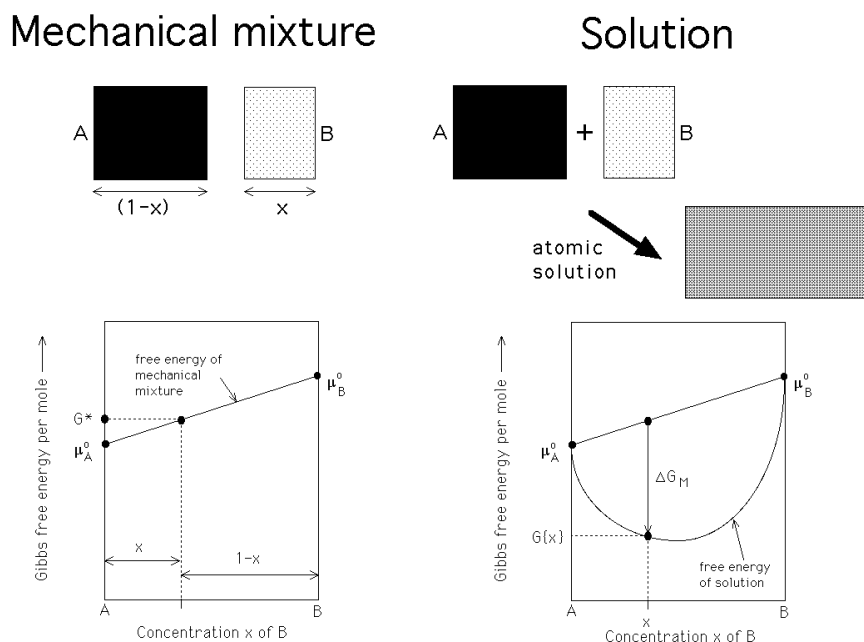


Fig. 4: (a) The free energy of a mechanical mixture, where the mean free energy is simply the weighted mean of the components. (b) The free energy of an ideal atomic solution is always lower than that of a mechanical mixture due to configurational entropy.

In contrast to a mechanical mixture, a *solution* is conventionally taken to describe a mixture of atoms or molecules. There will in general be an enthalpy change associated with the change in near neighbour bonds. Because the total number of ways in which the “particles” can arrange is now very large, there will always be a significant contribution from the entropy of mixing, even when the enthalpy of mixing is

zero. The free energy of the solution is therefore different from that of the mechanical mixture, as illustrated in Fig. 4b. The difference in the free energy between these two states of the components is the free energy of mixing  $\Delta G_M$ , the essential term in all thermodynamic models for solutions.

Whereas mechanical mixtures and atomic or molecular solutions are familiar in all of the natural sciences, the intermediate states have only recently been addressed. The problem is illustrated in Fig. 5 which shows the division of particles into ever smaller particles until an atomic solution is achieved. At what point in the size scale do these mixtures of particles begin to exhibit solution-like behaviour?

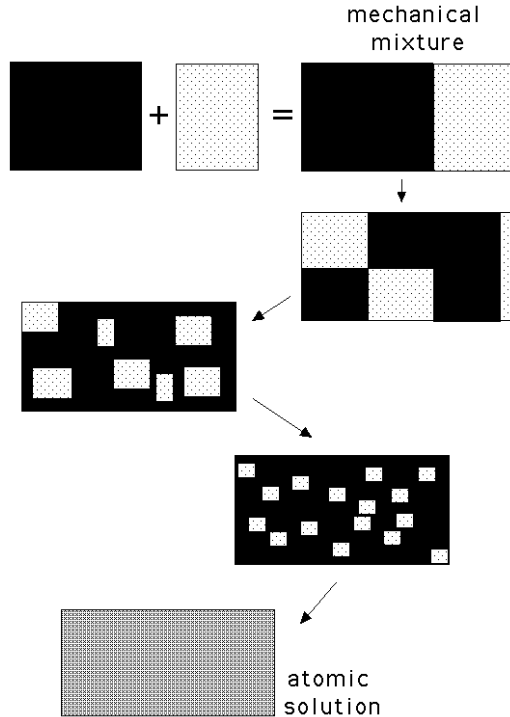


Fig. 5: Schematic illustration of the evolution of an atomic solution by the progressive reduction in the size of different particles, a process akin to mechanical alloying.

To answer this question we shall assume first that there is no enthalpy of mixing. The problem then reduces to one of finding the configurational entropy of mixtures of lumps as opposed to atoms. Suppose that there are  $m_A$  atoms per powder particle of  $A$ , and  $m_B$  atoms per particle of  $B$ ; the powders are then mixed in a proportion which gives an average mole fraction  $x$  of  $B$ .

There is only one configuration when the heaps of pure powders are separate. When the powders are mixed at random, the number of possible configurations for a mole of atoms becomes:

$$\frac{(N_a([1-x]/m_A + x/m_B))!}{(N_a[1-x]/m_A)! (N_ax/m_B)!} \quad (2)$$

where  $N_a$  is Avogadro's number. The numerator in equation 2 is the total number of particles and the denominator the product of the factorials of the  $A$  and  $B$  particles respectively. Using the Boltzmann equation and Stirling's approximation, the molar entropy of mixing becomes:

$$\begin{aligned} \frac{\Delta S_M}{kN_a} = & \frac{(1-x)m_B + xm_A}{m_A m_B} \ln \left\{ N_a \frac{(1-x)m_B + xm_A}{m_A m_B} \right\} \\ & - \frac{1-x}{m_A} \ln \left\{ \frac{N_a(1-x)}{m_A} \right\} \\ & - \frac{x}{m_B} \ln \left\{ \frac{N_a x}{m_B} \right\} \end{aligned} \quad (3)$$

subject to the condition that the number of particles remains integral and non-zero. As a check, it is easy to show that this equation reduces to the familiar

$$\Delta S_M = -kN_a[(1-x) \ln\{1-x\} + x \ln\{x\}] \quad (4)$$

when  $m_A = m_B = 1$ .

Naturally, the largest reduction in free energy occurs when the particle sizes are atomic. Fig. 6 shows the molar free energy of mixing for a case where the average composition is equiatomic assuming that only configurational entropy contributes to the free energy of mixing. An equiatomic composition maximises configurational entropy. When it is considered that phase changes often occur at appreciable rates when the accompanying reduction in free energy is just  $10 \text{ J mol}^{-1}$ , Fig. 6 shows that the entropy of mixing cannot be ignored when the particle size is less than a few hundreds of atoms. In commercial practice, powder metallurgically produced particles are typically  $100 \mu\text{m}$  in size, in which case the entropy of mixing can be neglected entirely, though for the case illustrated, solution-like behaviour occurs when the particle size is about  $10^2$  atoms.

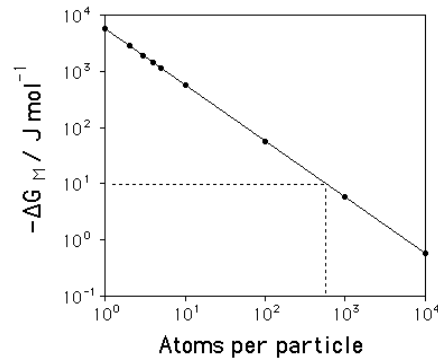


Fig. 6: The molar Gibbs free energy of mixing,  $\Delta G_M = -T\Delta S_M$ , for a binary alloy, as a function of the particle size when all the particles are of uniform size in a mixture whose average composition is equiatomic.  $T = 1000 \text{ K}$ .

## Enthalpy and Interfacial Energy

The enthalpy of mixing will not in general be zero as was assumed above. The binding energy is the change in energy as the distance between a pair of atoms is decreased from infinity to an equilibrium separation, which for a pair of  $A$  atoms is written  $-2\epsilon_{AA}$ . From standard theory for atomic solutions, the molar enthalpy of mixing is given by:

$$\Delta H_M \simeq N_a z(1-x)x\omega \quad \text{where} \quad \omega = \epsilon_{AA} + \epsilon_{BB} - 2\epsilon_{AB} \quad (5)$$

where  $z$  is a coordination number.

However, for particles which are not monatomic, only those atoms at the interface between the  $A$  and  $B$  particles will feel the influence of the unlike atoms. It follows that the enthalpy of mixing is not given by equation 5, but rather by

$$\Delta H_M = zN_a\omega \ 2\delta S_V \ x(1-x) \quad (6)$$

where  $S_V$  is the amount of  $A-B$  interfacial area per unit volume and  $2\delta$  is the thickness of the interface, where  $\delta$  is a monolayer of atoms.

A further enthalpy contribution, which does not occur in conventional solution theory, is the structural component of the interfacial energy per unit area,  $\sigma$ :

$$\Delta H_I = V_m S_V \sigma \quad (7)$$

where  $V_m$  is the molar volume.

Both of these equations contain the term  $S_V$ , which increases rapidly as the inverse of the particle size  $m$ . The model predicts that *solution formation is impossible* because the cost due to interfaces overwhelms any gain from binding energies or entropy. And yet, solutions do form, so there must be a mechanism to reduce interfacial energy as the particles are divided. The mechanism is the reverse of that associated with precipitation (Fig. 7). A small precipitate can be coherent but the coherency strains become intolerable as it grows. Similarly, during mechanical alloying it is conceivable that the particles must gain in coherence as their size diminishes. The milling process involves fracture and welding of the attrited particles so only those welds which lead to coherence might succeed.

Another unexpected result is obtained on incorporating a function which allows the interfacial energy to decrease as the particle size becomes finer during mechanical alloying. Thermodynamic barriers are discovered to the formation of a solution by the mechanical alloying process, Fig. 8. When the enthalpy of mixing is either zero or negative, there is a single barrier whose height depends on the competition between the reduction in free energy due to mixing and the increase in interfacial energy as the particles become finer until coherence sets in. When the atoms tend to cluster, there is a possibility of two barriers, the one at smaller size arising from the fact that atoms are being forced to mix during mechanical alloying.

The composition dependence of the barriers to solution formation becomes more clear in plot of free energy versus chemical composition, as illustrated in Fig. 8c,d.

## Shape of Free Energy Curves

There are many textbooks which emphasise that free energy of mixing curves such as that illustrated in Fig. 4b must be drawn such that the slope is either  $-\infty$  or  $+\infty$  at

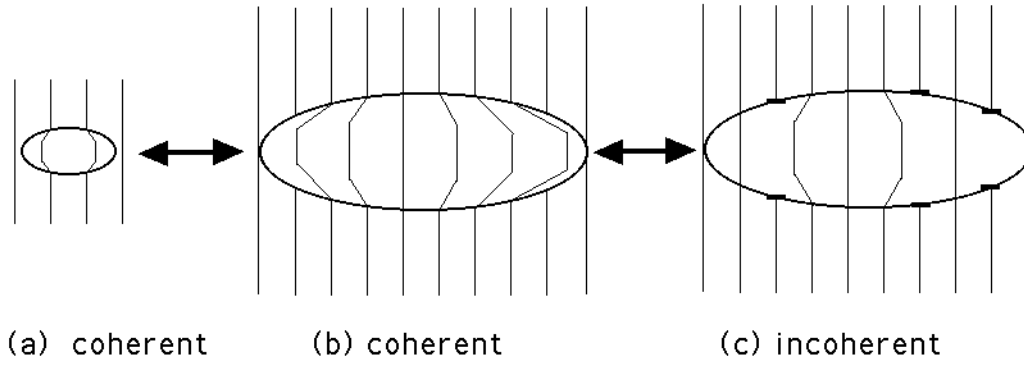


Fig. 7: The change in coherence as a function of particle size. The lines represent lattice planes which are continuous at the matrix/precipitate interface during coherence, but sometimes terminate in dislocations for the incoherent state. Precipitation occurs in the sequence a→c whereas mechanical alloying is predicted to lead to a gain in coherence in the sequence c→a.

$x = 0$  and  $x = 1$  respectively. This is a straightforward result from equation 4 which shows that

$$\frac{\partial \Delta S_M}{\partial x} = -kN_a \ln \left\{ \frac{x}{1-x} \right\} \quad (8)$$

so that the slope of  $-T\Delta S_M$  becomes  $\pm\infty$  at the extremes of concentration. Notice that at those extremes, any contribution from the enthalpy of mixing will be finite and negligible by comparison, so that the free energy of mixing curve will also have slopes of  $\pm\infty$  at the vertical axes corresponding to the pure components† It follows that the free energy of mixing of any solution from its components will at first decrease at an infinite rate.

However, these conclusions are strictly valid only when the concentration is treated as a *continuous* variable which can be as close to zero or unity as desired. The present work emphasises that there is a *discrete* structure to solutions. Thus, when considering  $N$  particles, the concentration can never be less than  $1/N$  since the smallest amount of solute is just one particle. The slope of the free energy curve will not therefore be  $\pm\infty$  at the pure components, but rather a finite number depending on the number of particles involved in the process of solution formation. Since the concentration is not a continuous variable, the free energy “curve” is not a curve, but is better represented by a set of straight lines connecting the discrete values of concentration that are physically possible when mixing particles. Obviously, the shape approximates a curve when the number of particles is large, as is the case for an atomic solution made of a mole of atoms. But the curve remains an approximation.

---

† The intercepts at the vertical axes representing the pure components are nevertheless finite, with values  $\mu_A^0$  and  $\mu_B^0$ .

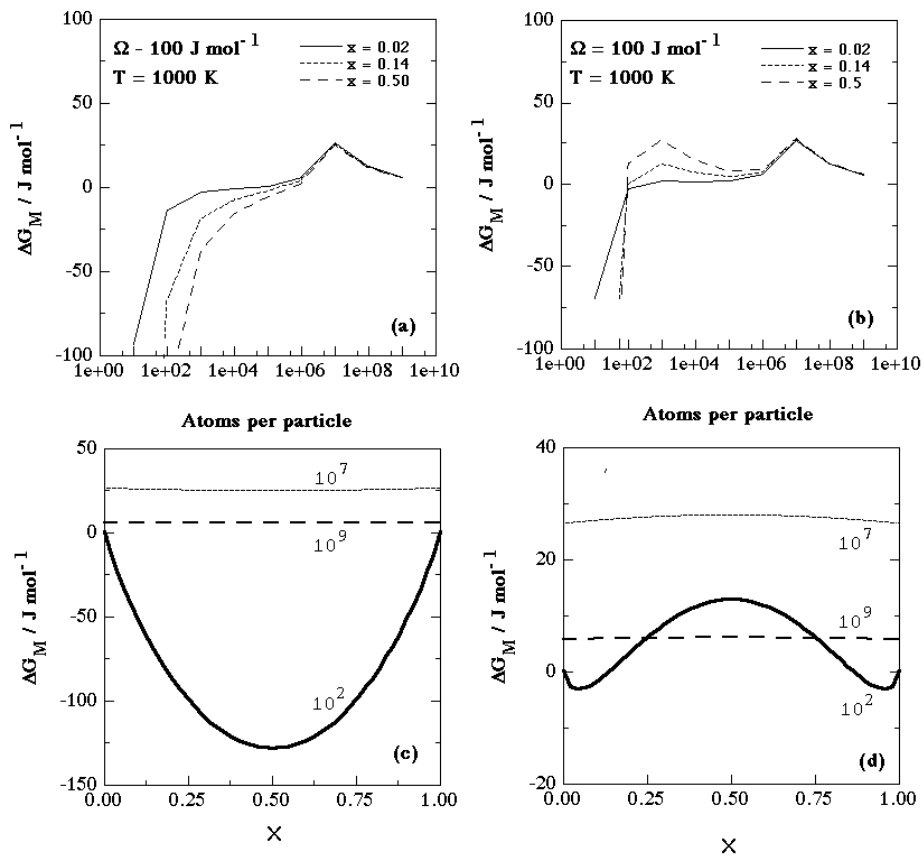


Fig. 8: Thermodynamic barriers to solution formation. (a) Case where the enthalpy of mixing is negative, *i.e.* unlike atoms attract. (b) Case where there is a tendency to cluster with a positive enthalpy of mixing. (c) As case (a) but plotted against chemical composition. The numbers alongside the curves refer to the number of atoms per particle. (d) As case (b) but plotted against chemical composition. The numbers alongside the curves refer to the number of atoms per particle.

# Recrystallisation of Practical Mechanically Alloyed Iron–Base and and Nickel–Base Superalloys

Materials Science and Engineering A223 (1997) 64-77

H. K. D. H. Bhadeshia  
University of Cambridge/JRDC  
Department of Materials Science and Metallurgy  
Pembroke Street, Cambridge CB2 3QZ, U.K.

## Abstract

Commercialised mechanically alloyed yttria dispersion strengthened alloys exhibit unusual recrystallisation behaviour. In spite of their large stored energy content, they tend to recrystallise at temperatures close to melting. The recrystallised microstructure is often very coarse and highly anisotropic, characterised by columnar grains. Such a microstructure is often referred to as being “directional recrystallised”. This and other features of these unique alloys are reviewed. It is found that many of the observed peculiarities can be attributed to the ultra-fine grained structure present prior to the recrystallisation heat-treatment. In some cases the manufacturing process tends to align the dispersoid particles along the principal fabrication direction. This in turn encourages recrystallisation to be directional.

## INTRODUCTION

Some of the most successful mechanically alloyed materials include the oxide dispersion strengthened iron–base and nickel–base superalloys. Their recrystallisation behaviour is peculiar and is the subject of this review. During heat treatment of the consolidated mechanically alloyed (MA) powders, the bulk samples recrystallise into remarkably anisotropic and coarse columnar grain structures. In addition, recrystallisation usually does not occur until temperatures close to melting are reached [1–3].

The mechanical alloying process itself has been reviewed elsewhere [1–4]. Briefly, it involves the creation of an alloy by the intense mechanical deformation of mixtures of elemental or master–alloy powders (Fig. 1). The powders are then consolidated by various combinations of hot–isostatic pressing and extrusion; the alloys in this condition are usually too hard to use. They are therefore heat–treated, either isothermally or in a temperature gradient to induce recrystallisation. Mechanical alloying permits the usual limits of solubility imposed by solidification to be exceeded, but in addition, dispersoid particles (such as oxides) can be introduced uniformly into bulk materials. It is this latter facility which has led to commercial exploitation on a large scale. The mechanical alloying process is a relatively difficult manufacturing method. Variations in processing conditions (which are seldom revealed) can completely change

the subsequent properties of the alloys. For this reason, we concentrate here on alloys which are considered to be established commercially and which therefore should have reproducible properties.

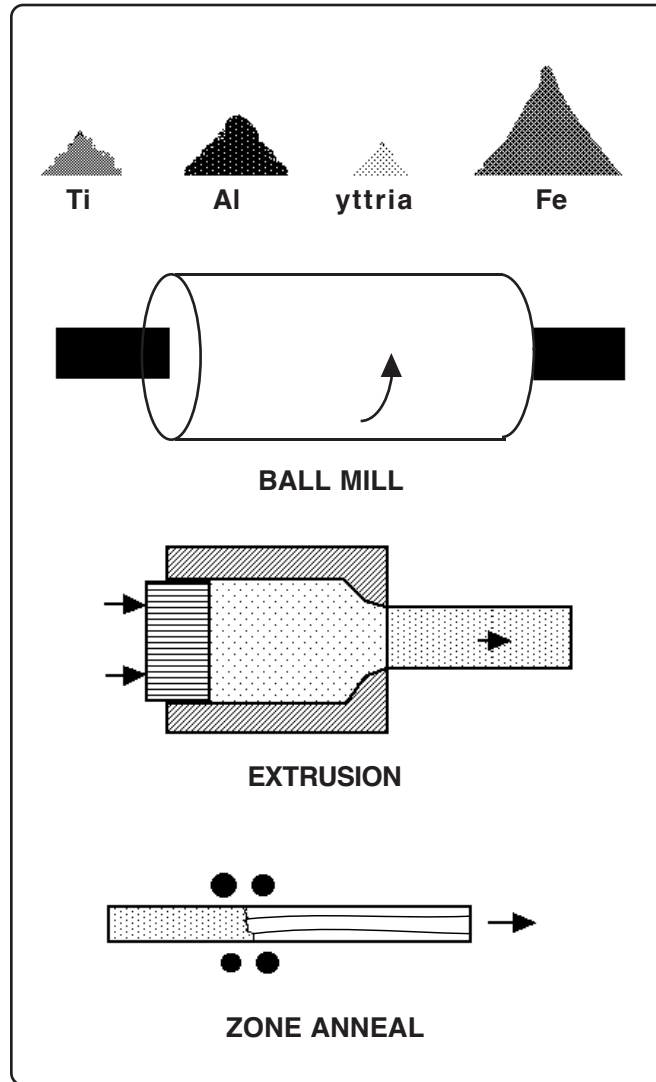


Fig. 1: A schematic illustration of a common method of manufacturing large quantities of mechanically alloyed metals for engineering applications. The elemental powders/master-alloys/oxides are milled together to produce solid solutions with oxide dispersoids. This powder is then consolidated and the resulting bulk alloy heat-treated to achieve a coarse, directional grain structure.

This review begins with an introduction to the range of important commercial alloys, followed by an assessment of their strange recrystallisation behaviour. There are two main classes of mechanical alloys which are of commercial significance, the oxide dispersion strengthened

Steels	C	Cr	Al	Mo	Ti	N	Ti <sub>2</sub> O <sub>3</sub>	Y <sub>2</sub> O <sub>3</sub>	Fe	
MA957	0.01	14.0	–	0.3	1.0	0.012	–	0.27	Balance	
DT2203Y05		13.0	–	1.5	2.2		–	0.5	Balance	
ODM 331		13.0	3.0	1.5	0.6		–	0.5	Balance	
ODM 751		16.5	4.5	1.5	0.6		–	0.5	Balance	
ODM 061		20.0	6.0	1.5	0.6		–	0.5	Balance	
MA956	0.01	20.0	4.5	–	0.5	0.045	–	0.50	Balance	
PM2000	< 0.04	20.0	5.5		0.5		–	0.5	Balance	
PM2010	< 0.04	20.0	5.5		0.5		–	1.0	Balance	
DT		13.0	–	1.5	2.9		1.8	–	Balance	
DY		13.0	–	1.5	2.2		0.9	0.5	Balance	
Ni–Base	C	Cr	Al	Ti	W	Fe	N	Total O	Y <sub>2</sub> O <sub>3</sub>	Ni
MA6000	0.06	15.0	4.5	2.3	3.9	1.5	0.2	0.57	1.1	Balance
MA760	0.06	19.5	6.0	–	3.4	1.2	0.3	0.6	1.0	Balance
MA758 †	0.05	30.0	0.3	–	0.5	–	–	0.37	0.6	Balance

Table 0: Compositions (wt.% ) of some typical alloys. † MA758 is a nickel base mechanical alloy without  $\gamma'$  strengthening. The compositions of ODM061, DT and DY are from Regle [5], as are the nitrogen data for MA956 and MA957. The compositions of PM2000 and PM2010 are from Krautwasser *et al.* [6].

(ODS) iron–base superalloys and the ODS nickel–base superalloys †.

### *Iron–Base Alloys*

These alloys (Table 1) are designed to be oxidation and corrosion resistant, but with a greater creep strength when compared with equivalent cast alloys, due to the dispersion of fine yttria particles. MA956 has the greater oxidation resistance due to the higher chromium

---

† The following trade names are used throughout the text: MA956, MA957, MA6000 and MA760 are alloys manufactured by INCO; the ODM series, DT and DY are alloys manufactured by Dour Metal (the term *ODM* originates from the phrase *oxide dispersion strengthened microforged*). The alloy DT2203Y05 has been developed by CEN/SCK of Belgium; PM2000 and PM2010 are alloys developed by Plansee of Austria (they were during the development stage also known by the designations F10 and F11 respectively).

concentration, and its large aluminium content. The presence of yttria suppresses the spalling of the protective alumina films by trapping sulphur at the particle/matrix interfaces and hence reducing its segregation to the oxide/metal interface [Ikeda *et al.*, 1995]. All of the steels listed are supposed to be ferritic. Normal ferritic steels tend to undergo a marked loss in creep strength at temperatures in excess of 600 °C; the ODS alloys discussed here can in principle be used at much higher temperatures.

The ferritic state also makes the iron–base alloys less susceptible to radiation induced swelling. MA957 and a similar steel DT2203Y05 are therefore designed for nuclear reactor applications, for use in a liquid sodium environment at temperatures of the order of 700 °C. Both have a high void swelling resistance, and a low carbon concentration in order to avoid the formation of titanium carbides. The titanium is meant to combine with chromium, molybdenum and iron to form a stable b.c.c. FeCrTiMo intermetallic  $\chi$ –phase during ageing at around 800 °C, which can further boost the creep strength. The rupture strength of ODM751 is larger than that of MA956 [7]. ODM751 has an additional 1.5 wt.% Mo which, either via the  $\chi$ –phase or through solid solution strengthening, presumably adds to the creep strength of ODM751. However, the results are confusing because PM2000, which does not contain molybdenum, virtually matches the rupture strength of ODM751.

#### *Nickel–Base Alloys*

The nickel–base alloys MA6000 and MA760 are both  $\gamma'$  strengthened, as in conventional nickel–base superalloys; the dispersion strengthening with yttria allows the strength to be maintained to much higher temperatures. For example, at 1093 °C, the 1000 hour rupture strength of MA6000 is twice that of conventional nickel–base superalloys. For reasons which are not clear, the (low and high cycle) fatigue resistance of MA6000 is much better than that of conventional alloys, as is its thermal fatigue resistance [2].

A lot of the oxidation resistance of MA6000 relies on the formation of chromia at the surface. However, chromia is not very resistant to sulphidation. Resistance to sulphide attack is important in industrial gas turbine manufacture, where the ODS alloys have applications as vanes. MA760 has a higher sulphidation and oxidation resistance, due to its higher chromium and aluminium concentrations, the latter inducing the formation of surface alumina [8].

The reported solidus temperatures and densities of some of the alloys are listed in Table 2. Similar data do not seem to be available in the published literature for the other alloys listed in Table 1. There is nothing unusual in these data, but they are relevant in two respects. Firstly, it will be seen later that the recrystallisation temperatures of both the iron and nickel base alloys are generally close to the temperature at which melting begins. Secondly, the

mechanical alloying and subsequent consolidation process leads to a density which cannot, within the limits of experimental error, be distinguished from that obtained by conventional casting and solidification.

Alloy	Solidus Temperature / °C	Density g cm <sup>-3</sup>	References
MA956 (Fe base)	1482	7.2	INCO datasheet
MA956 (Fe base)		7.12	Regle [5]
MA957 (Fe base)	≈ 1500	7.62	Regle [5]
MA758 (Ni base)	1350	8.14	Sha & Bhadeshia [9] INCO datasheet
MA760 (Ni base)	1295	7.89	Sha & Bhadeshia [9] INCO datasheet
MA6000 (Ni base)	1296	8.11	INCO datasheet

Table 2: Some physical data for common alloys

## INITIAL MICROSTRUCTURES

Immediately after the mechanical alloying process, the powders are canned and extruded/hot-rolled to produce the appropriate bulk forms of the alloys. The as-mechanically alloyed materials have a grain size which can be as fine as 1–2 nm locally. During heating for either extrusion or rolling, the canned mechanically alloyed powders may recrystallise to a sub-micron grain size which is representative of the grain structure found immediately after consolidation (Fig. 2). These incredibly fine grain sizes are a consequence of the strains imparted on the powders during the mechanical alloying process, true strains of the order of 9 (equivalent to stretching a unit length by a factor of 8000). The subsequent consolidation by comparison involves minor degrees of deformation, but much higher bulk temperatures (around 1000 °C). It is known that during the course of consolidation, the material may dynamically recrystallise several times. It should be emphasized that the sub-micron grains referred to above are true grains with large relative misorientations, not simply dislocation cell structures generated by deformation.

Nevertheless, the iron-base alloys immediately after consolidation have a cold-deformed microstructure in which the ultra-fine grains are elongated along the working direction and contain other classic features of cold work, *i.e.* the high dislocation density and a generally convoluted microstructure. The dislocation density has been measured for DT2203Y05 to be about  $10^{15} \text{ m}^{-2}$  [10]; although this is large, it is not particularly high when compared with dislo-

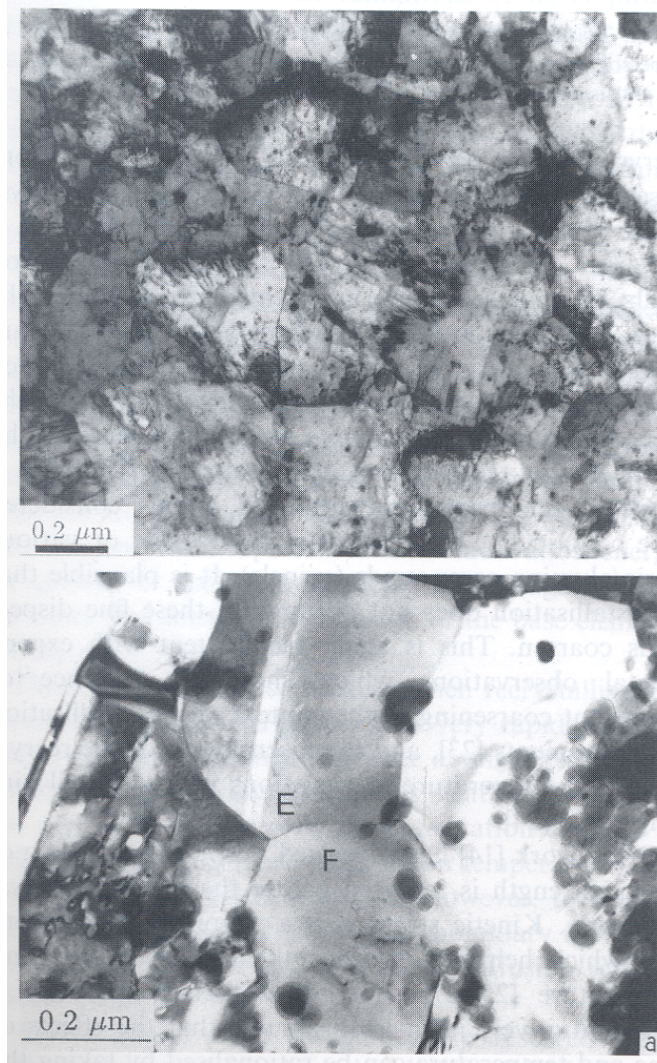


Fig. 2: Transmission electron micrographs showing the sub-micron grain structure of mechanically alloyed and consolidated alloys. (a) Iron-base MA956. (b) Nickel-base MA6000; electron diffraction confirms that there are large misorientations across grains such as  $E$  and  $F$ . The grains in both cases do not represent low-misorientation cells of the type common in ordinary deformation. Both micrographs are sections normal to the extrusion direction. The appearance of MA6000 microstructure is independent of the plane of section, but the microstructure of MA956 is cold-deformed and hence the grains are elongated along the extrusion direction.

cation densities found in conventional steel martensitic microstructures (Fig. 3a). Subsequent heat-treatment leads to primary recrystallisation into a very coarse grained microstructure (Fig. 3b).

The nickel-base superalloys also have an ultra-fine grained microstructure, but one which is the product of primary recrystallisation (Fig. 2b). The sub-micrometer grains are therefore equiaxed, contain undistorted annealing twins and a clean microstructure. Subsequent heat treatment therefore leads to secondary recrystallisation driven by the grain boundary energy of the fine grained primary recrystallised state. It is not clear why the nickel base alloys are in a primary recrystallised state following extrusion/hot-rolling, whereas the iron-base alloys,

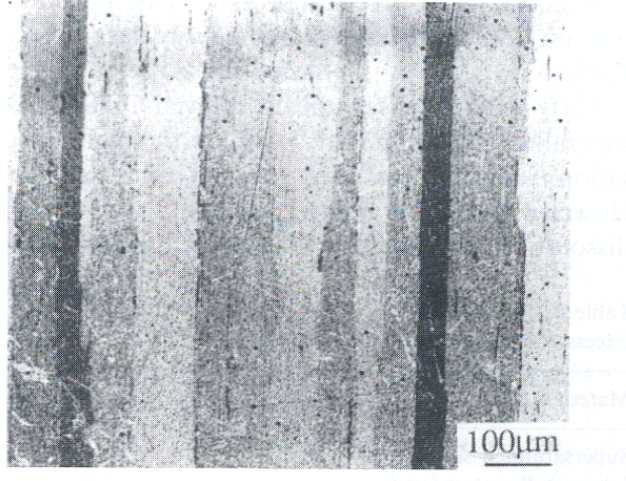
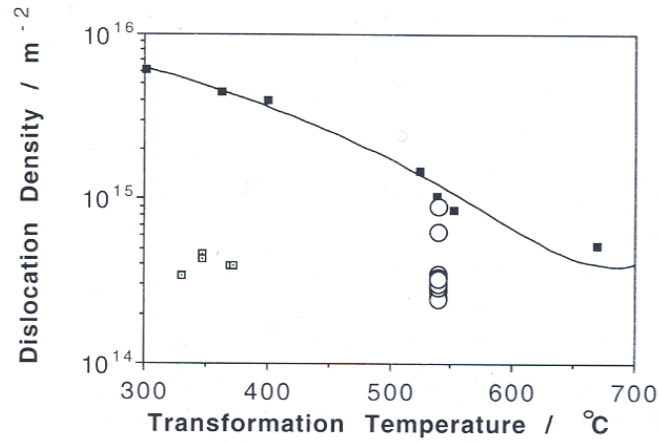


Fig. 3: (a) The measured dislocation densities as a function of the transformation temperature in low-alloy steels. The microstructures range from Widmanstätten ferrite, bainite, acicular ferrite and martensite [11,12]. (b) An optical micrograph showing a typical directionally recrystallised grain structure. The alloy concerned is MA956, but the microstructure is broadly representative of all of the alloys listed in Table 1.

which are fabricated under identical conditions, have a cold deformed microstructure.

Irrespective of whether the alloys have a primary or secondary recrystallised microstructure, the ultra-fine grains obtained after recrystallisation make the alloys very hard (Table 3) and for most applications unusable without heat treatment which leads to an enormous coarsening of the microstructure with a reduction in the amount of grain surface per unit volume by 2-3 orders of magnitude. The details of recrystallisation are discussed in the next section.

The excess energy stored in the mechanically alloyed and consolidated materials described in Table 1 is primarily in the form of grain surfaces and to a lesser extent due to dislocations and other high-entropy defects. We shall see later that this stored energy amounts to about

Alloy	HV, Before Recrystallisation	HV, After Recrystallisation
MA957	400–410	230–240
MA956	350–390	225–245
MA956 Sheet	410	250
MA6000	645	500–520
MA760	720–790	500–515
MA758	405	214

Table 3: Typical Vicker’s Hardness data before and after recrystallisation into a coarse grained microstructure.

$1 \text{ J g}^{-1}$  in spite of the sub-micron grain size. Although this value is much larger than that in normal cold-deformed materials, it is much smaller than in many metastable materials. This is because the commercial alloys do not contain more solute than can be tolerated by the matrix – the mechanical alloying process is not used commercially to trap excess solute, but primarily to introduce stable oxide dispersions. Table 4 lists the excess energies of some metastable materials in units of  $RT_M$ , where  $R$  is the gas constant and  $T_M$  the absolute melting temperature. Thus, a unit value corresponds approximately to the thermal energy available at the melting temperature. It is evident that the commercial alloys are not particularly metastable in this context.

Materials Example	$RT_M$ units
Supersaturated Solution	$< 1$
Intermetallic Compounds	$< 0.5$
Amorphous Solids	$< 0.5$
Compositionally Modulated Films	$< 0.1$
Interphase Dispersions	$< 0.1$
Commercial Mechanical Alloys	$< 0.005$

Table 4: Excess energy in metastable materials. Some of the data are from Turnbull [13]. The supersaturated solution is one in which solute has been trapped against equilibrium.

Extrusion/rolling leads to an alignment of dispersoid particles along the working direction, the degree of alignment being pronounced in the case of the iron-base alloys [14] Fig. 4. This alignment reflects inhomogeneities in the fabrication process arising at the single particle level

and below. Thus, the iron–base alloys almost always tend to recrystallise into a columnar grained microstructure, with the principal growth direction being parallel to the extrusion direction, irrespective of whether the sample is zone annealed, cross annealed or isothermally treated. (Cross annealing is zone annealing along a direction normal to the extrusion direction). For reasons which are not clear, the anisotropy in particle dispersion is much less for the nickel base superalloys, in which the direction of columnar grain growth can often be controlled by the sense of the temperature gradient during zone annealing. Indeed, equiaxed coarse grained secondary recrystallised microstructures can be readily generated either by isothermal annealing or by zone annealing at high speeds [15].

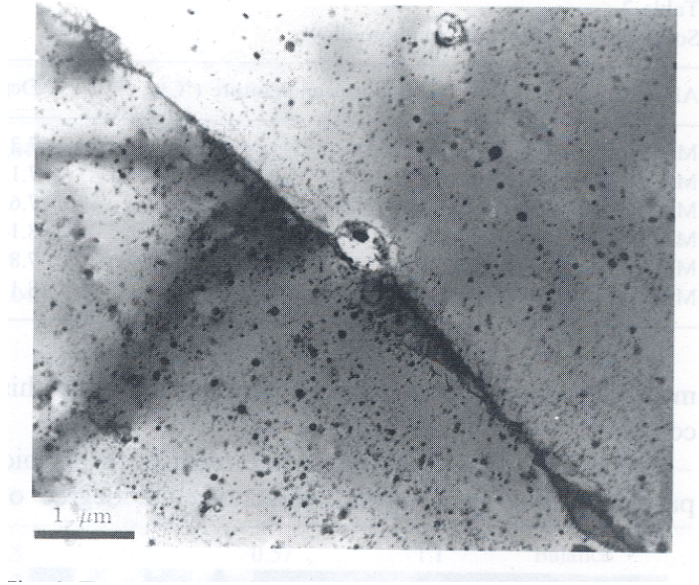


Fig. 4: Transmission electron micrograph showing the alignment of dispersoid particles in MA956. The rows of particles are parallel to the extrusion direction identified by the grain boundary

### THE RECRYSTALLISATION TEMPERATURE

The recrystallisation of mechanically alloyed yttria dispersion strengthened steels and nickel–base superalloys occurs at exceptionally high homologous temperatures, of the order of 0.9 of the melting temperature ( $T_M$ ). This contrasts with recrystallisation at about 0.6  $T_M$  in ordinary variants of similar metallic alloys. Strangely enough, the mechanically alloyed metals contain a more stored energy than in conventional materials which recrystallise at lower temperatures; recrystallisation normally is accelerated as the stored energy increases. Some measured stored energy data are listed in Table 5.

Alloy	Stored Energy $\text{J g}^{-1}$	Heating Rate $\text{K min}^{-1}$	Comment
MA957	1.0		Primary Recrystallisation
MA956	0.4		Primary Recrystallisation
MA956 sheet	$\simeq 0.4^\dagger$		
MA6000	0.6		Secondary Recrystallisation
MA760	1.0	30	Secondary Recrystallisation
MA758	0.3	10	Secondary Recrystallisation

Table 5: Enthalpy of Recrystallisation [9,16,17,18].  $\dagger$ : in MA956 sheet, the stored energy is released over a relatively large range of temperatures and is difficult to measure accurately. For MA758 the stored energy is small and recrystallisation occurs close to the melting point making the stored energy difficult to measure.

Early work on mechanically alloyed ODS nickel–base superalloys [19] tended to attribute the high recrystallisation temperatures the presence of  $\gamma'$  precipitates. However, there are many such alloys for which the  $\gamma'$  dissolution temperature is well below that at which recrystallisation occurs [20,21,22]. Furthermore, the iron–base alloys do not contain any  $\gamma'$  and yet also recrystallise at similarly high temperatures.

It has been speculated [23] that recrystallisation might be initiated when at elevated temperatures the grain boundary mobility suddenly rises because grain boundary solute drag effects are overcome at elevated temperatures. This is inconsistent with the fact that the recrystallisation temperature can be altered greatly by relatively low–temperature heat treatments [16].

All of the mechanically alloyed metals considered here contain fine particles of yttrium oxide or various yttria/alumina compounds (spinels). It is plausible that recrystallisation does not occur until these fine dispersoids coarsen. This is again inconsistent with experimental observations which show the absence of significant coarsening in the context of recrystallisation heat treatments [24], and the insensitivity of the recrystallisation temperature to variations in the overall pinning force [25].

Other work [15] has suggested that a critical value of kinetic strength is required before the onset of recrystallisation. Kinetic strength is a simple empirical concept which helps to combine the effects of time and temperature [26,27,28]. For an isothermal process, it seems

intuitively justified to assume that the effects of time and temperature can be rationalised by taking the product:

$$t \exp\{-Q/kT\} \quad (1)$$

where  $t$  is the heat treatment time,  $Q$  is an activation energy and the other terms have their usual meanings. This concept can be generalised to anisothermal heat treatments by taking the integral:

$$\int \exp\{-Q/kT\{t\}\} dt \quad (2)$$

over the cycle of interest. Although the method has been successful within the limitations of its empirical character, it fails to explain the unexpectedly high recrystallisation temperatures in the mechanically alloyed metals. The activation energy  $Q$  needed in the kinetic strength function, to rationalise available data on any particular alloy turns out to be some ten times greater than that for the self diffusion of the base element.

More fundamental methods of analysing overall transformation kinetics are based on the Johnson–Mehl–Avrami method, which can be developed to as much rigour as is necessary, or as the need to know certain parameters permits. One simplification often used is to ignore nucleation by assuming that a fixed number of nucleation sites exists at time zero. If this is done for the mechanical alloys, then the experimental data are only well represented if the activation energy for growth is made unrealistically large (again, some ten times that for the self diffusion of the base element) [25,29].

These difficulties arise because when recrystallisation occurs at around  $0.9 T_M$ , it occurs very rapidly during isothermal heat treatment, or over a very narrow temperature range during continuous heating. Such data can only be represented by large activation energies in order to achieve high recrystallisation temperatures and rapid subsequent transformation. However, to assume that the activation energy for grain boundary motion is very much greater than that for self-diffusion ( $Q_D$ ) is unconvincing.

Almost all of these difficulties are resolved when nucleation is considered in detail [29,30]. It turns out that the activation energy for *nucleation* in the mechanical alloys should indeed be very large. This is because the alloys have an unusually small grain size prior to recrystallisation. The nucleation of recrystallisation occurs by the bowing of grain boundaries, a process which for conventional alloys is straightforward since the distance between grain boundary junctions is usually larger than between other strong pinning points. With the sub-micrometer grain size of mechanically alloyed metals, the grain junctions themselves act as severe pinning lines for grain boundary bowing (Fig. 5). It is easy to demonstrate that this should lead to an

enormous activation energy for the nucleation of recrystallisation, many orders of magnitude larger than  $Q_D$ . It should be noted that  $Q$  in this model might be reduced if a few grains happen to be slightly larger than others (either because adjacent grains are similarly orientated or because of local variations due to the uncertainties in the mechanical alloying process).

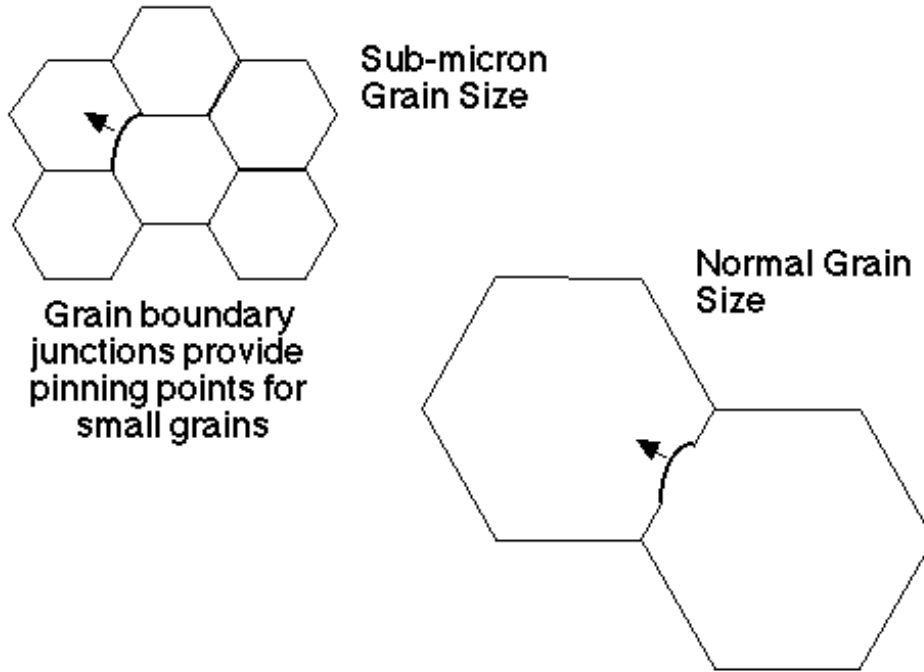


Fig. 5: The nucleation of recrystallisation occurs by the formation of a grain boundary bulge. This can occur with less constraint when the grain junctions are spaced at distances greater than the critical bulge size. With the ultra-fine grains of mechanically alloyed metals, the grain junctions are themselves pinning points, making it very difficult to form large enough bulges.

This model for nucleation suggests a new concept, that individual grains cannot be considered to be topologically independent when the grain size becomes sufficiently small. It has some remarkable consequences which have been verified experimentally:

- (a) The model explains the high homologous recrystallisation temperatures irrespective of alloy system. Recrystallisation is retarded whenever the grain size is small enough for the grain junctions to act as pinning points during the formation of viable nuclei in the form of grain boundary bulges.
- (b) The model predicts that the recrystallisation temperature should decrease if the the stored energy is reduced by a low-temperature heat treatment which leads to uniform grain

coarsening. This has now been verified experimentally for several alloys [16,29]. Since recrystallisation should eventually become more difficult as the stored energy is reduced, the curve of recrystallisation temperature versus grain size (or stored energy) should show a minimum. This prediction has been verified experimentally [29].

## ROLE OF CRYSTALLOGRAPHIC TEXTURE

Studies of the effect of the crystallographic texture in consolidated MA ODS alloys on their recrystallisation behaviour have been confined to the iron–base alloys. There is conclusive evidence that the recrystallisation temperature can be sensitive to the initial texture. A reasonable explanation for this is that grain boundary mobility is affected by texture. During the directional recrystallisation of ultra–fine grained MA ODS alloys, the recrystallised grains are usually several hundreds of microns in width, and advance into a matrix with sub–micrometer sized grains. Thus, the recrystallisation front in effect “sees” a tremendous variety of crystallographic orientations and might be regarded as advancing into a liquid like structure. It then is reasonable that samples in which the grains are oriented high mobility along the extrusion direction, recrystallise more readily.

Crystallographic texture data suggest that when there is a preferred distribution of orientations, the major components of texture in the mechanically alloyed steels are  $\{001\} \langle 110 \rangle$ ,  $\{111\} \langle \bar{1}10 \rangle$  [31,32], which belong to the so–called  $\alpha$  and  $\gamma$  fibres in crystal orientation distribution space. This applies in both the states, before and after recrystallisation, the recrystallisation process simply changing the strength of the texture components with respect to a random distribution of orientations. For reasons which are not obvious, recrystallisation seems easiest whenever the  $\{111\} \langle \bar{1}10 \rangle$  is prominent (Table 6). Thus, MA956 prior to recrystallisation is rich in this particular component whereas MA957 is not, probably due to the presence of austenite in MA957 at the fabrication temperature [16]. The former has a substantially lower recrystallisation temperature compared with the latter, even though MA957 has a relatively higher stored energy and lower yttria content than MA956. However, if MA957 is pre–annealed (*i.e.* heat–treated without recrystallisation) in order to make its texture comparable to that of MA956, then its recrystallisation temperature drops in spite of the reduction in stored energy due to the preannealing heat–treatment.

Evens *et al.* [33] have also conducted microtextural measurements, and interpreted their recrystallisation results in terms of the different mobilities of grain boundaries with different orientations.

To summarise, there is no doubt that texture can influence the recrystallisation charac-

	As-Received MA956	As-Received MA957	Preannealed MA957
Stored Energy $J g^{-1}$	0.4	1.00	0.70
Recrystallisation Start	1273 °C	1429 °C	1362 °C
Recrystallisation Finish	1334 °C	1447 °C	1382 °C
Texture Summary	{111} < $\bar{1}10$ > {001} < 110 >	Random Random	{111} < $\bar{1}10$ > {001} < 110 >
Recrystallised Grains	Highly anisotropic	anisotropic	Equiaxed fine

Table 6: Recrystallisation characteristics of MA956 and MA957 in the as-received condition [17]

teristics, but the mechanism remains unclear. There are many data in the literature which show that the stored energy varies with the texture components, but those data are not relevant in the present context because contrary to the results of conventional recrystallisation experiments, the reduction in recrystallisation temperature is accompanied by a reduction in stored energy. It could be argued that the particular component {111} <  $\bar{1}10$  > gives a higher grain boundary mobility within a liquid-like matrix of ultra-fine grains, but this explanation remains speculative.

### THE DISPERSOIDS AND PRECIPITATES

Fine yttria particles ( $\simeq 10$  nm) are incorporated into the metallic matrix as a consequence of the ball milling operations. Most of these survive as yttrium oxide in spite of consolidation by extrusion and rolling at about 1050 °C. However, heat-treatment causes these particles to react with dissolved aluminium (or titanium) and oxygen to produce a variety of compounds [6,25,34,35]. The possible combinations of yttria and alumina include those listed in Table 7.

$3Y_2O_3 \cdot 5Al_2O_3$	YAG	yttrium aluminium garnet
$Y_2O_3 \cdot Al_2O_3$	YAH	yttrium aluminium hexagonal
$2Y_2O_3 \cdot Al_2O_3$	YAM	yttrium aluminium monoclinic
$Y_2O_3 \cdot Al_2O_3$	YAP	yttrium aluminium perovskite
$Y_2O_3 \cdot Al_2O_3$	YAP'	yttrium aluminium pseudo-perovskite
$3Y_2O_3 \cdot 5Al_2O_3$	YAT	yttrium aluminite tetragonal

Table 7: Yttrium-Aluminium-Oxygen compound reported to occur in mechanically alloyed ODS iron and nickel base alloys.

The alumina particles tend to be some 500 nm in size, the titanium carbonitrides about 100–200 nm in size [5], and both have a much smaller number density than the original yttria particles. Hence, the reaction does not lead to a significant coarsening of the size distribution or inter-particle spacing. Even extremely severe heat-treatment (72 hours at 1400 °C) has little effect on the yttrium containing particles [24]. Typical changes in the size of the finer particles are illustrated in Fig. 6, which represents data for samples annealed for 110 h at the temperatures indicated, for samples of PM2010 [6]. Note that these data do not represent coarsening driven by interface energy minimisation, but complicated effects originating in the reactions between the yttria, aluminium and oxygen. Thus, the volume fraction is not constant during heat treatment. The volume fraction of the smaller reactive particles increases, whereas any large alumina particles tend to dissolve as the aluminium reacts with the yttria [6].

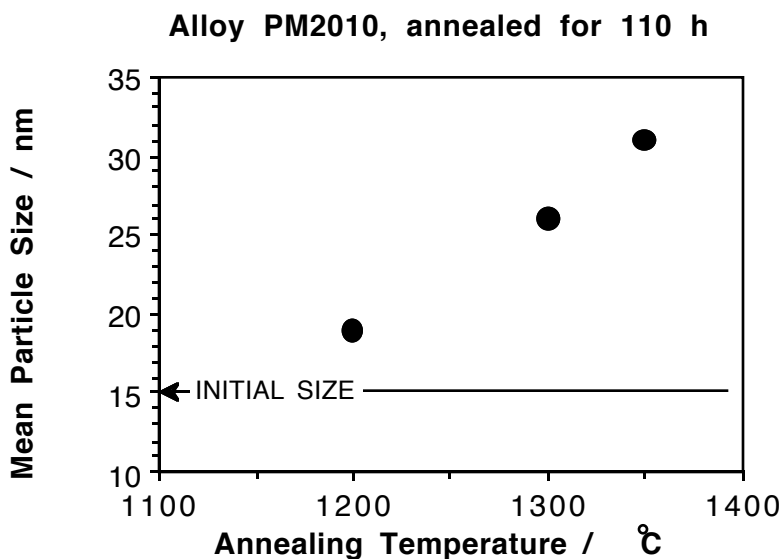


Fig. 6: Changes in particle size due to annealing, of alloy PM2010, for 110 h at each of the temperatures indicated. Data from Krautwasser *et al.* [6]

In the extruded condition, 80 % of the particles in both MA956 and MA957 are less than 15 nm in size, with those in MA956 being much smaller [5]. Nevertheless, the mean particle diameters are quite similar at 11.7 and 11.4 nm for MA957 and MA956 respectively [5], presumably because the fraction of particles is larger in the latter. Some typical particle sizes for the fine particles are presented in Table 8.

Almost all the mechanical alloys contain alumina particles introduced accidentally or as a consequence of internal oxidation during mechanical alloying (alumina is deliberately added to

Alloy	Mean Particle Size / nm	Reference
MA957	12	Regle [5]
MA956	12	Regle [5]
MA956	20	Hupalo <i>et al.</i> [**]
PM2010	15	Krautwasser <i>et al.</i> [6]

Table 8: Some particle characteristics, with the alloys in the unrecrystallised “as-received” condition.

ODM751 at the mechanical alloying stage). These particles are also stable, but are too coarse and few to cause significant Zener pinning. Titanium containing mechanical alloys such as MA957 and MA6000 also contain titanium-rich particles whose exact character is not known; they may be oxides or carbo-nitrides.

The coarsest precipitates, which are not very stable, are the  $M_{23}C_6$  particles which are visible optically, and dissolve (at around 1000 °C) during heating to the recrystallisation temperature only to reprecipitate during slow cooling to ambient temperature. These carbides are found in the nickel-base superalloys and not in the iron-base alloys which contain very low carbon concentrations.

To summarise, the yttrium based dispersoids are extremely stable in spite of some reaction with aluminium and oxygen to form garnets. The other particles are likely to be of little consequence to both the recrystallisation process and the creep resistance of the alloys.

The mechanism by which the fine yttrium containing particles enhance the creep resistance has been studied both for the mechanically alloyed nickel-base superalloys and the steels [36–39]. The creep resistance arises from the fact that dislocations have to climb over the hard obstacles. For steels, the consequent improvement in creep resistance allows alloys such as DT2203Y05 to be used at a service temperature of 975 K compared with that for conventional ferritic stainless steels whose maximum service temperature is about 925 K.

For the steels, there is some evidence that the oxide particles and the intermetallic compounds which precipitate in some alloys, inhibit the migration of boundaries (Evans *et al.*, 1992).

## EFFECT OF YTTRIA CONTENT

It might be assumed that an increase in the yttria content should lead to a corresponding increase in the creep resistance. This must be the case as the concentration is increased from zero, but recent work [6] indicates that there may be an optimum concentration of yttria. In a

series of experiments carried out on alloys PM2000 and PM2010, which differ only in the yttria content (0.5, 1.0 wt.% respectively), it was found that the higher yttria content of PM2010 does not lead to a significantly larger number density of fine dispersoids ( $< 100$  nm). It was predicted therefore that PM2010 should not have a higher creep strength than PM2000 [6]. This result remains to be verified.

It also appears that in iron base alloys, yttria contents in excess of 0.5 wt.% cause a deterioration in oxidation resistance because of a change in the morphology of the oxide [41].

## THE GRAIN SHAPE

The major peculiar feature of the ODS mechanical alloys is that they tend to recrystallise into a highly anisotropic columnar grain structure. There are two reasons why such grain structures should arise. Zone annealing, like directional solidification can encourage growth along the associated moving temperature gradient. Secondly, any dispersoids may tend to align along the extrusion direction, so that the Zener pinning force is smallest for growth parallel to the working direction, for both MA957 and MA956.

The nickel base alloys do not have a pronounced nonuniform distribution of dispersoids. Thus, MA6000, when isothermally annealed, often recrystallises into an equiaxed grain structure (there are batch-to-batch variations). The same alloy will recrystallise directionally when zone annealed. The sense of the columnar grains can be altered by changing the zone annealed direction; cross annealing (*i.e.* zone annealing in a direction normal to the extrusion direction) causes the growth of stubby columnar grains normal to the extrusion direction, confirming a more or less uniform dispersoid distribution. In addition, zone annealing at high speeds leads to a transition from a columnar to equiaxed recrystallised grains [15].

The nickel base alloy MA760 has a response which is similar to that of MA6000, although the signs are that there is a stronger alignment of particles along the extrusion direction. Thus, isothermal annealing does not lead to equiaxed grains, but cross annealing can change the direction of the columnar recrystallised grains.

The mechanically alloyed steels contain a very pronounced alignment of particles along the extrusion direction. Isothermal heat-treatment of as-worked samples always leads to the development of coarse columnar grains. MA957, which has a rather low yttria content, has relatively stubby columnar grains following isothermal heat treatment. No amount of cross annealing or any other heat treatment has succeeded in causing a change in the direction of columnar grain growth, which is always parallel to the working direction. The importance of a nonuniform dispersion of particles in inducing the development of columnar grains has been

emphasized in recent experiments where the introduction of HfC or TiB<sub>2</sub> led to the formation of anisotropic grains during secondary recrystallisation of the NiAl intermetallic matrix [42].

The roughness of grain boundaries in recrystallised mechanically alloyed nickel–base superalloys and steels has been characterised in detail [43–45]. The serrated boundaries arise because of transient pinning by dispersoids. Coarser and smoother boundaries occur when the stored energy is large, simply because it is then easier for the boundary to overcome the pinning force [45].

## PREANNEALING EFFECTS

Preannealing is a term used to describe a sample which has been heat treated at a temperature which is too low for recrystallisation, but high enough to induce significant changes in the stored energy, and in the subsequent microstructure following an elevated temperature recrystallisation heat treatment.

The effects of preannealing, at temperatures above that at which austenite can form, on MA957 can be summarised as follows [16]. A weak preannealing treatment (at about 1150 °C) has little or no effect on subsequent recrystallisation. As the preannealing time is increased, there is a transition from a coarse columnar grain structure to one which is equiaxed (20–40 μm) depending on the exact heat treatment). This is because the reduction in stored energy reduces grain boundary mobility, so that nucleation has an opportunity to develop in several regions of the sample, giving an equiaxed grain structure.

Continued preannealing causes the development of a bimodal equiaxed grain structure. This is because there is an inhomogeneous distribution of pinning particles in the alloy. The now substantial reduction in stored energy due to preannealing, retards recrystallisation more in some regions compared with others which are less strongly pinned. For MA957 the preannealing time at 1150 °C is in excess of 160 hours for this condition to be reached.

Further preannealing leads to such a large reduction in the stored energy that subsequent recrystallisation is suppressed.

It is much more difficult to control the grain structure of MA956 using preannealing heat treatments. Grain refinement certainly occurs, as in MA957, but the fine grains tend not to be equiaxed. This may be because MA956 contains a larger concentration of yttria. The anisotropic pinning due to the inhomogeneous distribution of the oxide particles is more difficult to overcome if the fraction of particles is large. It would be very interesting to test this with MA956 containing a smaller quantity of yttria dispersoids.

## VOID SWELLING RESISTANCE: FERRITIC ALLOYS

The formation of voids during irradiation causes the swelling of metals. A discussion of such effects is included here for interest. Irradiation tends to cause the formation of both interstitials and vacancies in equal concentrations, but the former anneal out more rapidly than the latter. The resulting excess vacancy concentration can condense out to form voids.

The subject has been reviewed by Little [46]. It seems that ferritic steels have a much higher resistance to void swelling than austenitic alloys, although nickel base alloys rank alongside the ferritic steels. Point defects introduced by irradiation can condense at *neutral* or *biased* sinks. The latter are typically dislocations with large Burgers vectors and attract more interstitials than vacancies, leaving an excess of vacancies to form voids. Hence, anything which encourages neutral sinks makes for a high void swelling resistance.

It is believed that in ferritic steels, irradiation induces two kinds of dislocations, one which is strongly biased and the other which is neutral. Hence there are effective sinks for both interstitial and vacancy point defects, thereby leading to a smaller excess of vacancies capable of forming voids.

However, there are significant variations in the void swelling resistance over the range of available creep resistant ferritic steels. For a given vacancy concentration, a larger number density of vacancy traps is conducive to a smaller tendency for swelling. Lath boundaries or the yttrium oxide particles in the mechanically alloyed steels are good vacancy traps. Hence, the latter alloys have very satisfactory void swelling resistance [46].

Some typical data comparing a mechanically alloyed ODS steel DT2203Y05 with a corresponding conventional ferritic steel AISI 410 (Fe-12Cr-0.4Ni-0.4Mn-0.2Si-0.1C wt.%) are given in Table 9 [10]. It is obvious that the mechanical alloy is able to accommodate a lot more helium and that it has a relatively high resistance to swelling. Little *et al.* found also that the matrix of the mechanically alloyed steel was stable to radiation-induced phase transformation; no changes were observed in the distribution of the chi-phase particles present before irradiation, although very fine scale effects could not be ruled out.

## NICKEL MODIFIED MA957

MA957 has a chemical composition which was originally formulated to ensure a ferritic microstructure for the sake of void swelling resistance during neutron irradiation. The Fe-Cr phase diagram shows a classical  $\gamma$ -loop *i.e.* the austenite phase field is enclosed in such a way that beyond a certain critical concentration, the ferrite remains the stable phase to the melting temperature. It has been discovered recently that the composition of conventional MA957 is

Alloy	Cavity	Cavity	Cavity	Dislocation
	Concentration	Diameter	Swelling	Density
	/ $10^{21} \text{ m}^{-3}$	/ nm	%	/ $10^{14} \text{ m}^{-2}$
DT2203Y05	8.0	8.3	0.24	9.7
AISI 410	19.8	6.0	0.49	8.9

Table 9: Results of experiments in which the samples were irradiated with chromium ions and  $\alpha$  particles to a total displacement dose of 50 dpa and a helium content of 600 appm [10]. The alloy DT2203Y05 was induction annealed at 1050 °C for 3 minutes, followed by ageing at 800 °C for 24 hours. It is not clear whether this heat treatment is sufficient to give a recrystallised microstructure.

such that it just clips the  $\gamma$ -loop at around 1000 °C, so that it is possible with suitable heat treatment to obtain a few percent of austenite [16].

Calculations have demonstrated that the addition of just  $\frac{1}{2}$  wt.% of nickel to the conventional alloy can raise the maximum austenite volume fraction to 0.5. Thus, a transformable mechanically alloyed steel, “MA957Ni” should be possible without any major changes in alloy chemistry.

Such alloys have now been made [47] and have confirmed the phase stability calculations. In fact, a series of four experimental alloys are available with a maximum austenite fraction from 0-1. The transformations have been detected experimentally. The possibility of generating a variety of microstructures by transformation has also been demonstrated.

## COLD DEFORMATION

Regle and Alamo [48] have conducted extensive studies on the recrystallisation behaviour of MA956 and MA957, for samples which were cold deformed after extrusion. Two deformation processes were used, swaging and drawing, with reductions ranging from 10 → 60%.

Swaging and drawing led to quite different changes in crystallographic texture, and indeed to the subsequent recrystallisation behaviour. In all cases, deformation led to a reduction in the recrystallisation temperature, the change being largest for the cold-drawn samples. For MA957, the maximum reduction in the recrystallisation temperature was found to be about 200 °C from 1450 → 1250 °C. The corresponding maximum reduction for MA956 was for the cold drawn samples, where the recrystallisation temperature could be reduced from 1350 → 750 °C.

Chou [47] has measured the stored energies in the samples studied by Regle and Alamo. Surprisingly, he found no increase in stored energy with deformation; indeed, it appears that

MA957	Recrystallisation Start, °C	Recrystallisation Finish, °C	Stored Energy J g <sup>-1</sup>
0% drawn	1370	1412	0.93
30% drawn	1018	1093	0.78
40% drawn	998	1056	0.70
50% drawn	989	1041	0.69
60% drawn	980	1027	0.65

Table 10: Cold drawn MA957. DSC measurements at 20 K min<sup>-1</sup> (after Chou, unpublished research)

the deformation leads to a reduction in stored energy (Table 10).

There is no clear explanation of the results, but it is possible that the cold deformation modifies the crystallographic texture. It is conceivable that the texture change both leads to a reduction in the stored energy, and at the same time, a reduction in the recrystallisation temperature. The texture could, for example, lead to the clustering of adjacent grains into similar orientations. This would lead to an increase in the effective grain size, thereby making the nucleation of recrystallisation more easy.

There are some other elegant results presented by Regle and Alamo, which are consistent with this interpretation. A sample which was necked by deformation (and hence contained a controlled deformation gradient), was subjected to a recrystallisation heat treatment. It was vividly demonstrated that the anisotropic recrystallisation grain structure became refined with the extent of deformation. This is in spite of the fact that the stored energy actually decreased. Thus, deformation must enhance the nucleation rate of recrystallisation, perhaps by the texture mechanism discussed above.

## TRANSFORMATION PLASTICITY

Phase transformation under the influence of an external stress can cause plasticity. This non-recoverable strain is not to be confused with creep; transformation plasticity can occur at temperatures and in time-scales which are wholly inconsistent with the generation of detectable creep strains.

MA957 is, within a restricted temperature range, able to transform to a few percent of austenite. However, modifications of MA957 which are able to transform to a much greater extent, are found to be much more susceptible to transformation-induced plasticity [49]. Applications in which these modified alloys undergo cyclic transformation under the influence of

stress are unlikely to be reliable.

## NONUNIFORM RECRYSTALLISATION

Most of the work in this area is on the nickel–base superalloy MA6000 [18]. It is found that there are profound differences across the cross section of the extruded bar, the edge regions recrystallising more easily relative to the core regions. The recrystallised grains tend to be have much larger aspect ratios at the edges. It appears that these differences are caused by inhomogeneous deformation. The oxide particles are more aligned along the extrusion direction at the regions near the surface, presumably because of the more extensive deformation in those regions. This alignment explains the greater anisotropy in the recrystallised grains and the relative ease of recrystallisation. The boundary mobility along the extrusion direction is larger when the particles are aligned. Stored energy measurements confirm that the observed effects cannot be explained by differences in the driving force for recrystallisation.

Martin [50] has discussed this work by presenting a calculation which indicates that the yttria particles, because of their small size, are not amenable to alignment by extrusion. However, Murakami *et al.* [51] have pointed out that his analysis assumes that the starting powder stock is uniform. This is not the case in practice. Mechanical alloying is a difficult process, and there are composition variations between powder particles/aggregates, which develop into banded regions as a consequence of extrusion. Results confirming the fact the mechanical alloying process can produce dispersoid inhomogeneities, which are carried through to the final product have recently been published by Jaeger and Jones [52,53] for alloys ODM 331 and ODM 751, both of which are iron based. This study is particularly useful in that the materials were examined both before and after consolidation. When a powder which is inhomogeneous in its dispersoid distribution is fabricated into a tube form, the particles align in concentric cylinders parallel to the tube axis. This in turn leads to an onion–peel type of recrystallised grain structure [53], which may be of some benefit from the point of view of mechanical properties.

It is strange that such inhomogeneities are most pronounced with the iron base alloys but not with the nickel base materials where the extent of particle alignment along the extrusion direction is usually minimal [16].

Finally, it is well established that both the manufacture of mechanically alloyed powder and the subsequent consolidation are both imperfect processes and lead to inhomogeneities in the final product. Fragments of improperly alloyed particles can be retained in the product, and act as defects [54]. If improperly bonded, they can act as cavities, or indeed as pinning centres for the advancing recrystallisation front.

## MA956 SHEET

MA956 sheet has the same composition as its rod form, but is made by a different route. After consolidating the mechanically alloyed powder by hot isostatic pressing, the billets are hot rolled with a reduction of approximately 98% to a thickness of 2.1 cm [55]. The rolling is carried out in the temperature range 1025–1065 °C.

The sheet is often cold deformed (typically another 60% reduction in thickness) before a recrystallisation heat treatment at about 1340 °C. The recrystallisation then begins at the centre of the sheet – in fact, the central regions tend to recrystallise completely before the surface regions [55]. The reason for such behaviour is not understood.

The crystallographic texture after the hot–deformation is  $\{100\} \langle 011 \rangle$ , a texture which is sharpened by deformation at ambient temperatures [55].

### RECRYSTALLISATION FRONT DUE TO ZONE ANNEALING

Directional recrystallisation during zone annealing can occur at a front which separates the recrystallised and unrecrystallised portions of the bar. The nature of the front has been characterised in MA6000 [56], in MA957 [14,33,57] and in MA956 [14]. Of these alloys, MA956 is exceptional in that the recrystallisation front is irregular (Fig. 7), extending over large distances along the zone annealing direction. The other alloys have a smooth recrystallisation front, which tends to be curved, the front advancing at a higher rate at the sample surface compared with the centre of the bar.

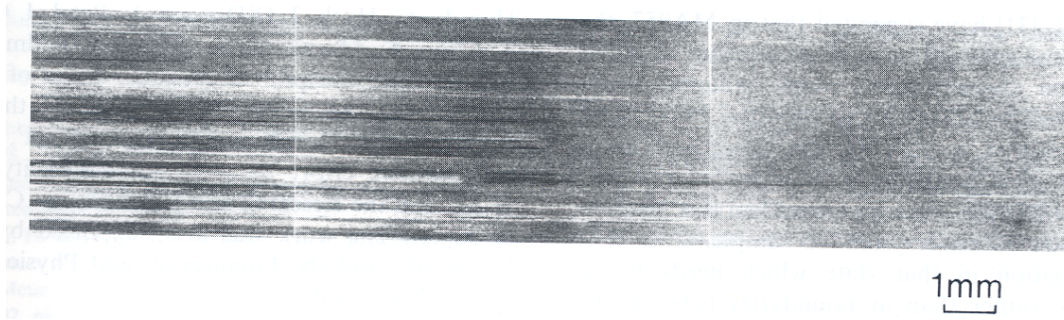


Fig. 7: An optical micrograph showing the spiked recrystallisation front of a partially recrystallised sample of MA956

There are a number of explanations for this curvature in the recrystallisation front. Heat penetrates through the surface so that the recrystallisation process at the surface should be

at a more advanced stage relative to the central regions. Miodownik *et al.* [57] carried out an experiment in which a partially zone annealed sample was subsequently held in a stationary temperature gradient for thirty minutes. Since the recrystallisation front remained curved, they claimed that the curvature cannot be explained by temperature gradients normal to the zone annealing axis. However, the degree of curvature in fact decreased on holding the sample in the stationary temperature gradient. The possibility therefore remains that temperature variations across the cross section of the bar are to some extent responsible for the curvature in the recrystallisation front.

In the specific case of a nickel–base superalloy MA6000, Murakami *et al.* [18] have shown that the extrusion process leads to a greater degree of dispersoid alignment in the surface regions of the bar, and that this leads to a greater ease of recrystallisation in those regions. This could also explain the curved recrystallisation front. By contrast, Marsh and Martin [56] ascribed the curved front to the existence of strain (and corresponding texture) gradients in the MA6000 bar. It is worth noting that although it is likely that the extrusion process leads to a greater degree of deformation in the surface regions, the stored energy of the MA6000 does not vary significantly across the cross–section [18] because the sample is in the primary recrystallised state before zone annealing.

Evens *et al.* [33] have suggested that in MA957, the curved recrystallisation front is a consequence of gradients in solute concentration, which influence grain boundary mobility. In support of this idea, Miodownik *et al.* [57] showed a peak in the concentration of titanium at a grain boundary in an extruded and heat treated bar of MA957. An experiment like this needs to be repeated on an unrecrystallised sample, since it is solute segregation in that state which needs to be characterised, rather than at boundaries between the coarse directionally recrystallised grain boundaries.

## COMPOSITE ALLOYS

Since MA956 is so heavily alloyed with aluminium and chromium, its ferritic matrix remains stable until the melting temperature. It is therefore not possible to control its grain structure using the  $\gamma \rightarrow \delta$  transformation. A feasible alternative could be to introduce a fraction of transformable material within the powder compact of MA956 before it is extruded. This amounts to making the alloy chemically inhomogeneous, a metallic composite dubbed MeMeC (metal–metal–composite). The transformable part can in principle help control the grain structure of the residue which does not transform.

Work in this area is in its early stages, but initial results show that it is possible to obtain

fine grained microstructures in MA956–20% MA957Ni composites.

## SUMMARY

Recrystallisation in MA–ODS iron and nickel–base alloys is dominated by the ultra–fine grain structure which is a consequence of the mechanical alloying and consolidation process, and by the presence of dispersoids. The grain structure can be so fine that the grain junctions themselves act to hinder the initiation of recrystallisation. Such fine grains cannot be considered to be topologically independent in this context. The dispersoids are mainly responsible for the anisotropy in the recrystallisation microstructure.

In general, the microstructure of these alloys is well–characterised and understood. It is necessary now to gain an equal understanding of the mechanical properties of such alloys.

## ACKNOWLEDGMENTS

The author is grateful to Professor A. H. Windle for the provision of laboratory facilities at the University of Cambridge and to Dr. David Gooch for commenting on several drafts of the paper. I am also grateful to H. Harada, G. Hack, J. O’Driscoll, L. Patel, J. O’Driscoll, T. Chou, K. Murakami, K. Mino, A. Badmos and W. Sha for many helpful discussions. Some of this work was carried out under the auspices of the “Atomic Arrangements: Design and Control Project”, which is a collaborative effort between the University of Cambridge and the Research and Development Corporation of Japan. The work was also supported by National Power plc. and the Engineering and Physical Sciences Research Council.

## REFERENCES

1. J. S. Benjamin and P. S. Gilman: *Metals Handbook*, ninth edition, ASM International, Ohio **7** (1983) 722.
2. G. H. Gessinger: *Powder Metallurgy of Superalloys*, Butterworth and Co., London. (1984)
3. G. A. J. Hack: *Powder Metallurgy* **27** (1984) 73–79.
4. J. S. Benjamin: *Metall. Trans.* **1** (1970) 2943–2951.
5. H. Regle: *Ph.D. Thesis*, “Alliages Ferritiques 14/20% de chrome Renforces par Dispersion d’Oxydes”, Universite de Paris–Sud. (1994)
6. P. Krautwasser, A. Czyrska–Filemonowic, M. Widera and F. Carsughi: *Materials Science and Engineering A* **A177** (1994) 199–208.
7. B. Kazimierzak, M. Prignon, C. Lecomte–Mertens and C. Coutsouradis: *High Temperature Materials for Power Engineering 1990*, Kluwer Academic Publishers, (1990) 131, quoted by Regle (1994).
8. L. Patel: *Private Communication*, to H. K. D. H. Bhadeshia, University of Cambridge, U. K. (1994)
9. W. Sha and H. K. D. H. Bhadeshia: *Metallurgical and Materials Transactions A* **25A** (1994) 705–714.
10. E. A. Little, D. J. Mazey and W. Hanks: *Scripta Metall. Mater.* **25** (1991) 1115–1118.
11. M. Takahashi and H. K. D. H. Bhadeshia: *Materials Science and Technology* **6** (1990) 592–603.
12. H. K. D. H. Bhadeshia: *Mathematical Modelling of Weld Phenomena III*, eds H. Cerjak and H. K. D. H. Bhadeshia, Institute of Materials, London (1996) in press.
13. D. Turnbull: *Metall. Trans. A* **12A** (1981) 695–708.
14. M. Baloch: *Ph.D. Thesis*, University of Cambridge. (1989)
15. M. Baloch and H. K. D. H. Bhadeshia: *Materials Science and Technology* **6** (1991) 1236–1246.
16. T. S. Chou and H. K. D. H. Bhadeshia: *Materials Science and Technology* **9** (1993) 890–897.
17. T. S. Chou and H. K. D. H. Bhadeshia: *Materials Science and Engineering A* **A189** (1994) 229–233.
18. K. Murakami, K. Mino, H. Harada and H. K. D. H. Bhadeshia: *Metall. Trans. A* **24A** (1993) 1049–1055.

19. Y. G. Nakagawa, H. Terashima and K. Mino: *Superalloys 1988*, eds S. Reichman, D. N. Duhl, G. Maurer, S. Antolovich and C. Lund, TMS-AIME, Warrendale, PA, U.S.A. (1988) 81–89.
20. K. Mino, Y. G. Nagakawa and A. Ohtomo: *Metall. Trans. A* **18A** (1987) 777.
21. K. Kusunoki, K. Sumino, Y. Kawasaki and M. Yamazaki: *Metall. Trans. A* **21A** (1990) 547.
22. K. Mino, H. Harada, H. K. D. H. Bhadeshia and M. Yamazaki: *Materials Science Forum* **88–90** (1992) 213–220.
23. P. Jongenburger: *Ph.D. Thesis no. 773*, Ecole Polytechnique Federale de Lausanne, Switzerland (1988)
24. A. P. Backhouse, S. S. Babu, K. Mino and H. K. D. H. Bhadeshia: *Pt. II Project Report*, Cambridge University. (1991)
25. K. Murakami: *Ph.D. Thesis*, Cambridge University. (1993)
26. J. H. Holloman and L. D. Jafee: *Trans. AIME* **162** (1945) 223–249.
27. P. J. Alberry and W. K. C. Jones: *Metals Technology* **4** (1977) 557–566.
28. M. F. Ashby and K. E. Easterling: *Acta Metall.* **30** (1982) 1969–1978.
29. W. Sha and H. K. D. H. Bhadeshia: *Materials Science and Engineering A* (1996) these proceedings.
30. K. Murakami and H. K. D. H. Bhadeshia: *Unpublished research*, Cambridge University. (1993)
31. A. Alamo, H. Regle and J. L. Bechade: *Novel Powder Processing*, Advances in Powder Metallurgy and Particulate Materials – 1992, Metal Powder Industries Federation, Princeton, NJ, USA **7** (1992) 169–182.
32. T. S. Chou and H. K. D. H. Bhadeshia: *Metall. Trans. A* **24A** (1993) 773–779.
33. P. J. Evens, J. W. Martin and E. A. Little: *Materials Science and Technology* **8** (1992) 531–536.
34. G. B. Schaffer, M. H. Loretto, R. E. Smallman and J. W. Brooks: *Acta Metall.* **37** (1989) 2551–2558.
35. H. Cama and T. A. Hughes: *Institute of Physics Conference Series No. 138: Section 7*, EMAG93, ed. A. Craven, IOP Publishing, Oxford, U. K. (1993) 361–364.
36. V. C. Nardone and J. K. Tien: *Scripta Metallurgica* **17** (1983) 467.
37. R. S. Herrick, J. R. Weertman, R. Petkovic–Luton, and M. J. Luton: *Scripta Metallurgica* **22** (1988) 1879.
38. J. H. Schroder and E. Arzt: *Scripta Metallurgica* **19** (1985) 1179.
39. J. Preston, B. Wilshire and E. A. Little: *Scripta Metall. Mater.* **25** (1991) 183–184.
40. R. W. Evans, J. Preston, B. Wilshire and E. A. Little: *J. of Nuclear Materials* **195** (1992) 24–28.
41. H. Nickel and W. J. Quadackers: *Heat Resistant Materials* eds. K. Natesan and D. J. Tillack, Fontana, WI, Sept. 1991, ASM International (1991) 87.
42. I.–G. Lee, A. K. Ghosh, R. Ray and S. Jha: *Metallurgical and Materials Transactions* **25A** (1994) 2017–2026.
43. D. L. Whittenberger: *Metallurgical Transactions A* **12A** (1981) 845.
44. D. M. Jaeger and A. R. Jones: *Materials for Combined Cycle Power Plant*, Institute of Metals, London (1991) 1–11.
45. K. Murakami, H. Harada and H. K. D. H. Bhadeshia: *Heat Treatment '92*, ed. I. Tamura, Kyoto, Japan (1992) 269–272.
46. E. A. Little: *Materials Modelling: From Theory to Technology*, IOP Publishing, Oxford (1991) 141–146.

47. T. S. Chou: *Ph.D. Thesis*, University of Cambridge. (1994)
48. H. Regle and A. Alamo: *Journal de Physique IV* **3**, **C7** (1993) 727–730
49. S. Suzuki and H. K. D. H. Bhadeshia: *Unpublished research*, Cambridge University. (1993)
50. J. W. Martin: *Metallurgical Transactions A* **25A** (1994) 651–652.
51. K. Murakami, K. Mino, H. Harada and H. K. D. H. Bhadeshia: *Metall. Trans. A* **25A** (1994) 652–653.
52. D. M. Jaeger and A. R. Jones: *Materials for Advanced Power Engineering*, “Dispersoid distributions in iron based ODS alloys made by mechanical alloying”, Leige, Belgium (1994) in press.
53. D. M. Jaeger and A. R. Jones: *Materials for Advanced Power Engineering*, “The development of grain shape in iron base ODS alloys”, Leige, Belgium (1994) in press.
54. D. M. Jaeger and A. R. Jones: *Processing, Properties and Applications of Metallic and Ceramic Materials*, eds. M. H. Loretto and G. J. Beevers, Birmingham, U. K. (1992) 1–6.
55. R. C. Klug, G. Krauss and D. K. Matlock: *Hot Deformation Textures and Microstructures*, TMS Fall Meeting, November 1993, Pittsburgh, PA, unpublished research. (1993)
56. J. M. Marsh and J. W. Martin: *Materials Science and Technology* **7** (1991) 183.
57. M. A. Miodownik, J. W. Martin and E. A. Little: *Journal of Materials Science Letters* **12** (1993) 834–835.
- . Y. Ikeda, H. Sumiyoshi and Y. Ishiwata: *ISIJ International* **35** (1995) 1109–1114.
- . Y. Kawasaki, Y. Ikeda, T. Kobayashi and H. Sumiyoshi: *ISIJ International* **36** (1996) 1208–1214.
- . M. F. Hupalo, M. Terada, A. M. Kliauga and A. F. Padilha: *Mat.-wiss. u. Werkstofftech.* **34** (2003) 505–508.